nature geoscience

SUPPLEMENTARY INFORMATION

DOI: 10.1038/NGEO2864

In the format provided by the authors and unedited.

Supercycle at the Ecuadorian subduction zone revealed after the 2016 Pedernales earthquake

J.-M. Nocquet[1*], P. Jarrin[2], M. Vallée[3], P. A. Mothes[2], R. Grandin[3], F. Rolandone[1,4], B. Delouis[1], H. Yepes[2], Y. Font[1], D. Fuentes[2], M. Régnier[1], A. Laurendeau[2], D. Cisneros[5], S. Hernandez[2], A. Sladen[1], J.-C. Singaucho[2], H. Mora[6], J. Gomez[5], L. Montes[5] , P. Charvis[1].

[1]Université Côte d'Azur, IRD, CNRS, Observatoire de la Côte d'Azur, Geoazur, Valbonne, France

[2]Instituto Geofísico, Escuela Politécnica Nacional, Quito, Ecuador

[3]Institut de Physique du globe de Paris, Sorbonne Paris Cité, Université Paris Diderot, UMR 7154 CNRS, Paris, France.

[4]Sorbonne Universités, UPMC Université Paris 06, CNRS, Institut des Sciences de la Terre de Paris (ISTeP), France.

[5]Instituto Geográfico Militar, Quito, Ecuador

[6]Servicio Geológico Colombiano, GNSS GeoRED Project, Center for Processing and Analysis of Geodetic Data, Bogotá, Colombia

correspondence to: nocquet@geoazur.unice.fr

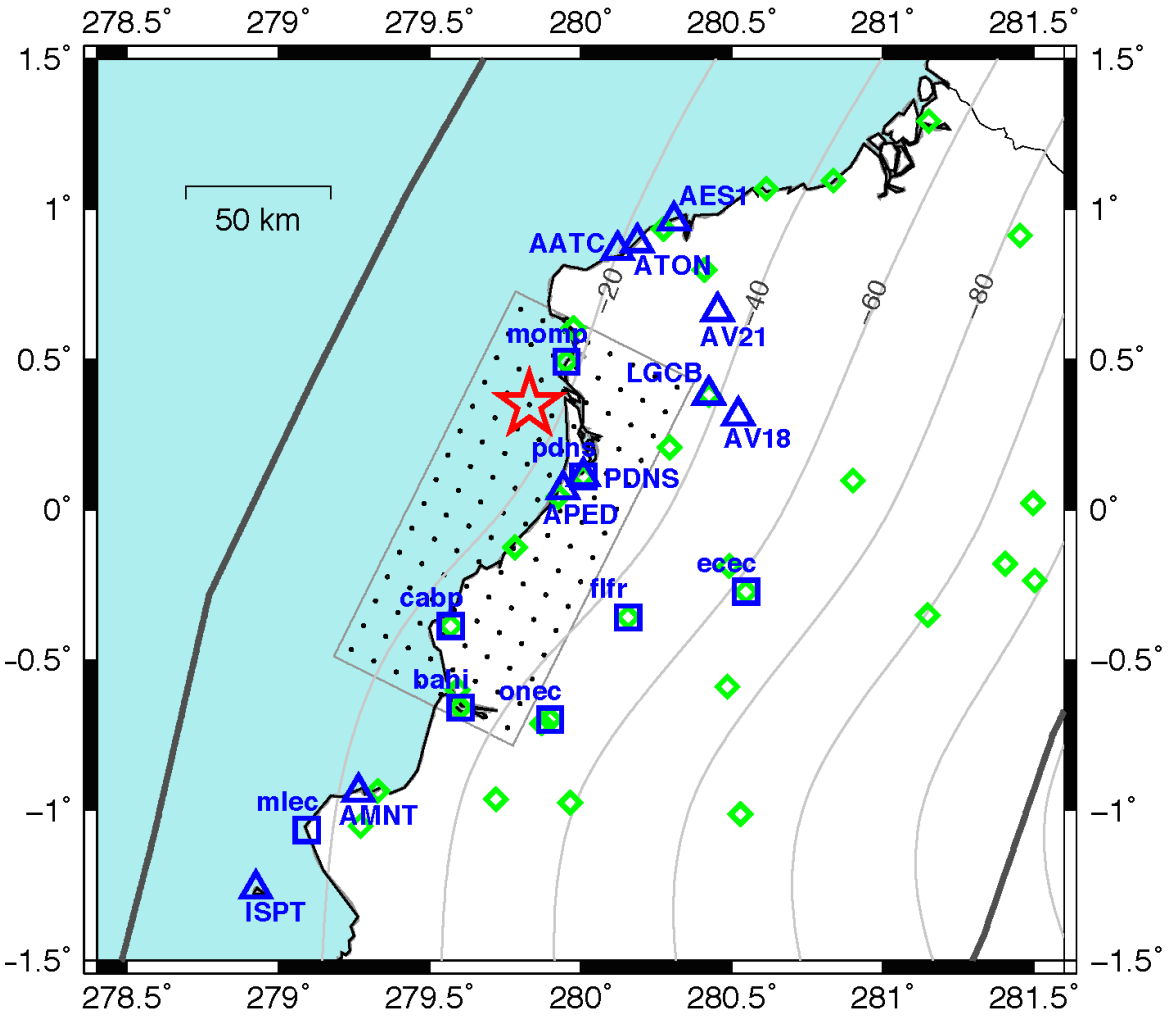

Supplementary Figure 1 | Near field data used in the kinematic slip inversion. Green diamonds, blue squares and blue triangles are the static GPS, HRGPS and accelerometric stations, respectively. Upper case name are accelerometers data, lower case name for HRGPS. The epicentre location is indicated by the red star. The fault geometry and its discretization (black dots) are shown together with iso-depth every 20 km from the SLAB1.0 model[1].

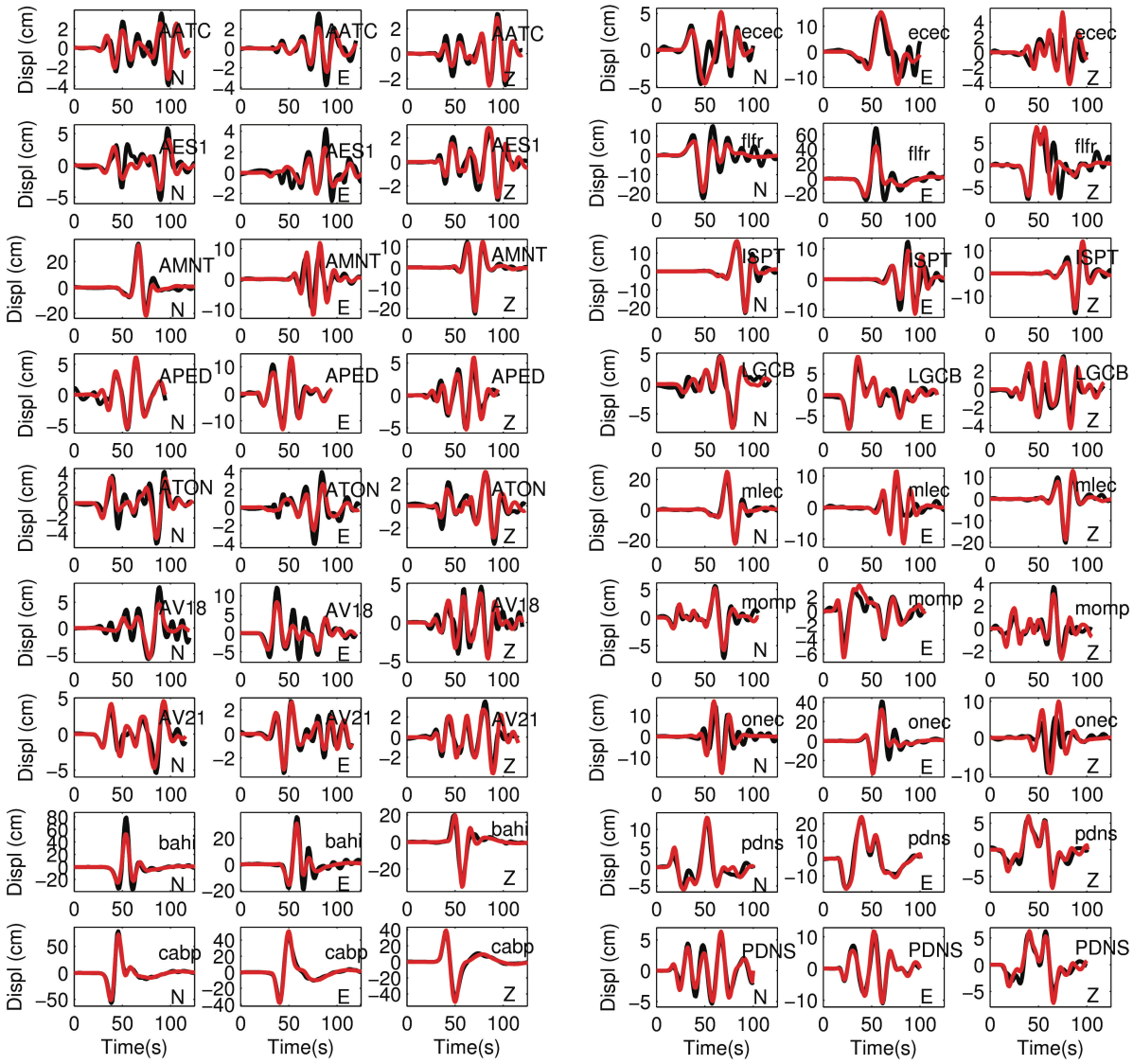

Supplementary Figure 2 | Observed and models local ground motions. Three-component data (black) and synthetics (red) are lowpass filtered in displacement at 0.08Hz. The highpass filter is 0.015Hz for the HRGPS stations and varies between 0.04Hz and 0.015Hz for the accelerometric stations depending on the noise level. Station name (Supplementary Fig. 1) and component are indicated in each sub-figure.

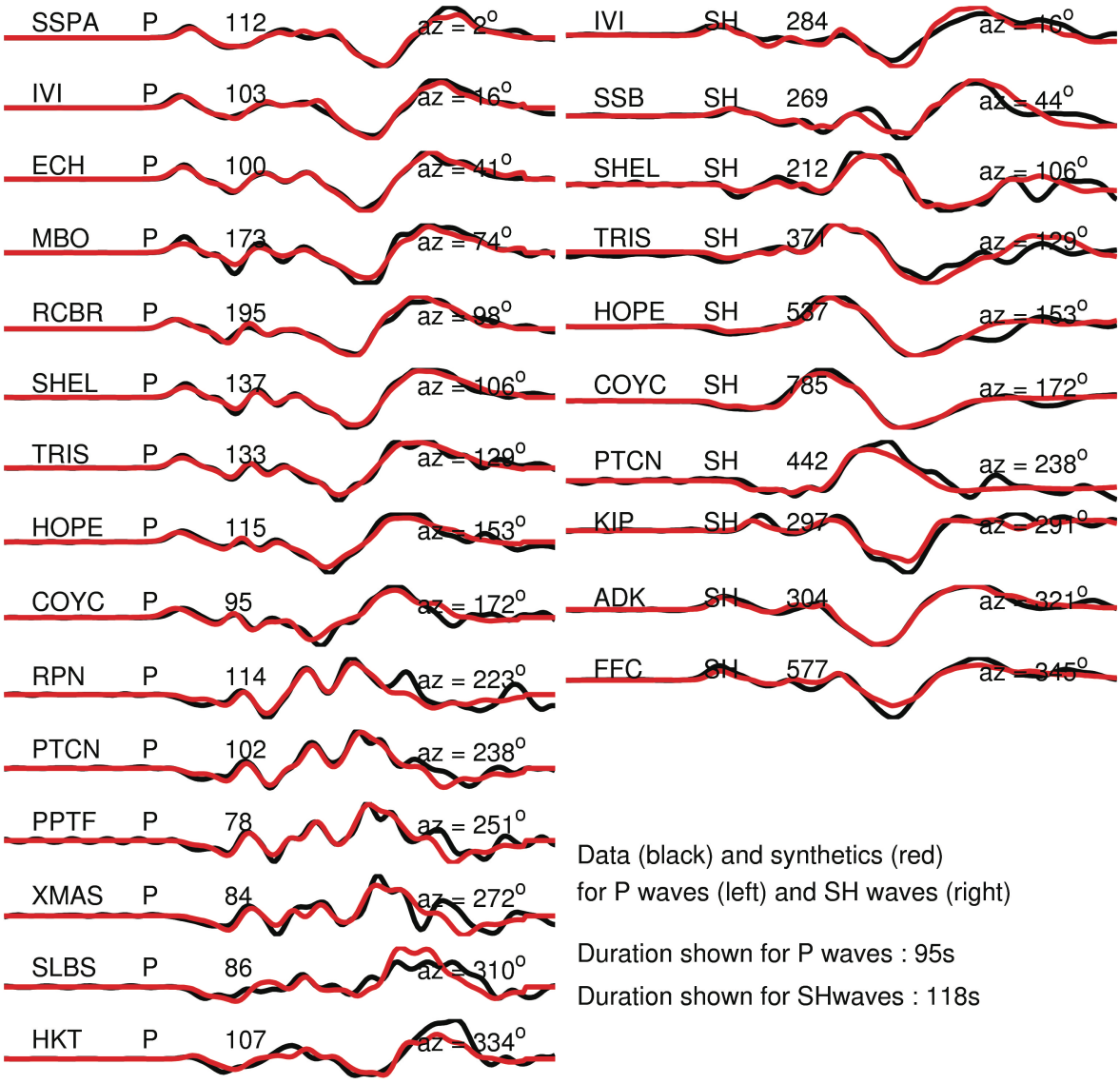

Supplementary Figure 3 | Teleseismic body waves modeling. Data (black) and synthetics (red) are filtered in displacement between 0.005Hz and 0.25Hz. For each station, its name, wave type, peak amplitude in μm, and azimuth are indicated.

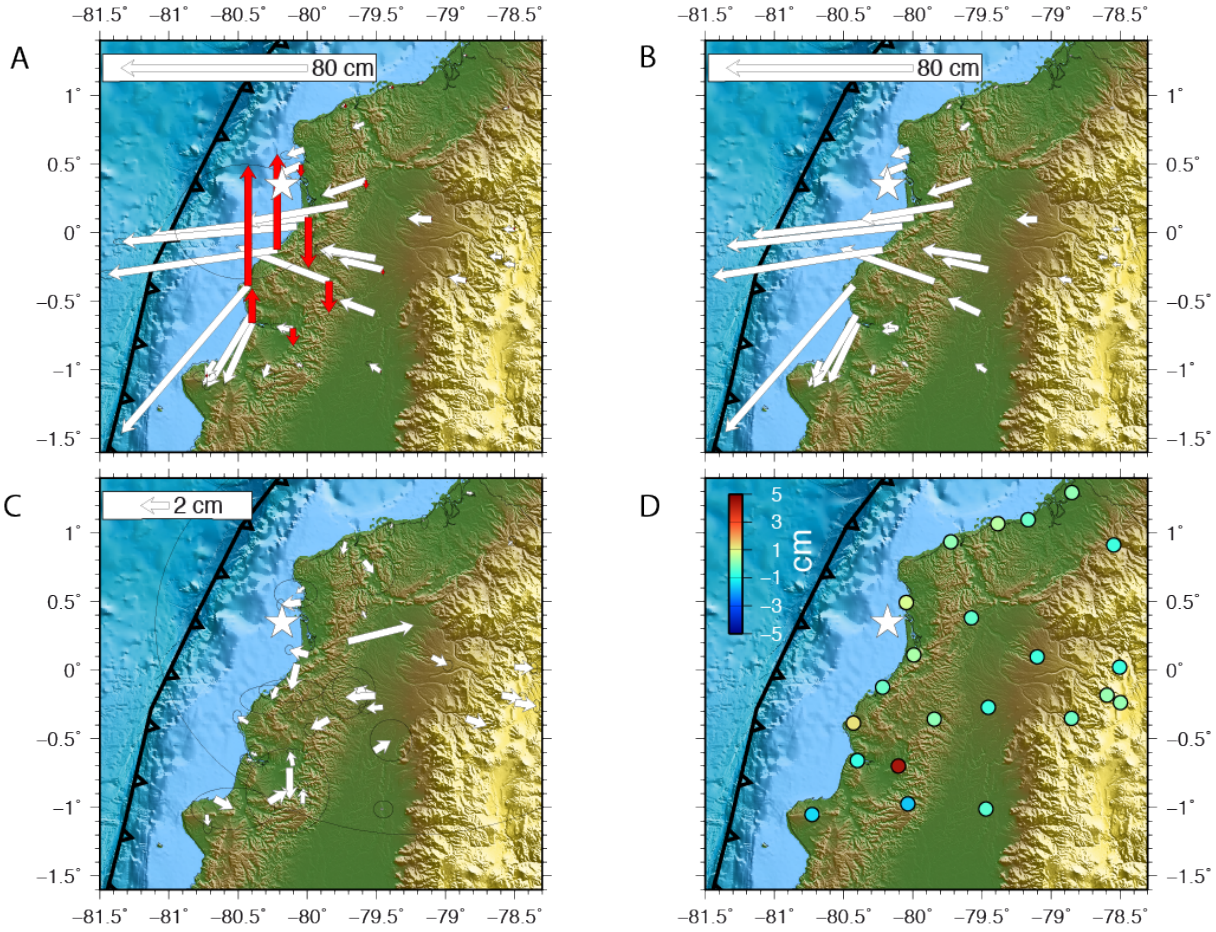

Supplementary Figure 4 | Comparison between observed and modelled coseismic static displacement from GPS. (A) Observed horizontal (white) and vertical (red) static co-seismic displacement (B) Predicted coseismic horizontal static displacements. (C) Residuals (Observed - Predicted) horizontal displacement. (D) Vertical residual (Observed - Predicted) displacements. The arrow is the top-left inset indicates the scale of displacement for each figure. The color-coded scale in (D) indicates the magnitude of residual vertical displacements. The white star marks the epicentre of the 2016 earthquake. The black line with triangles shows the location of the trench.

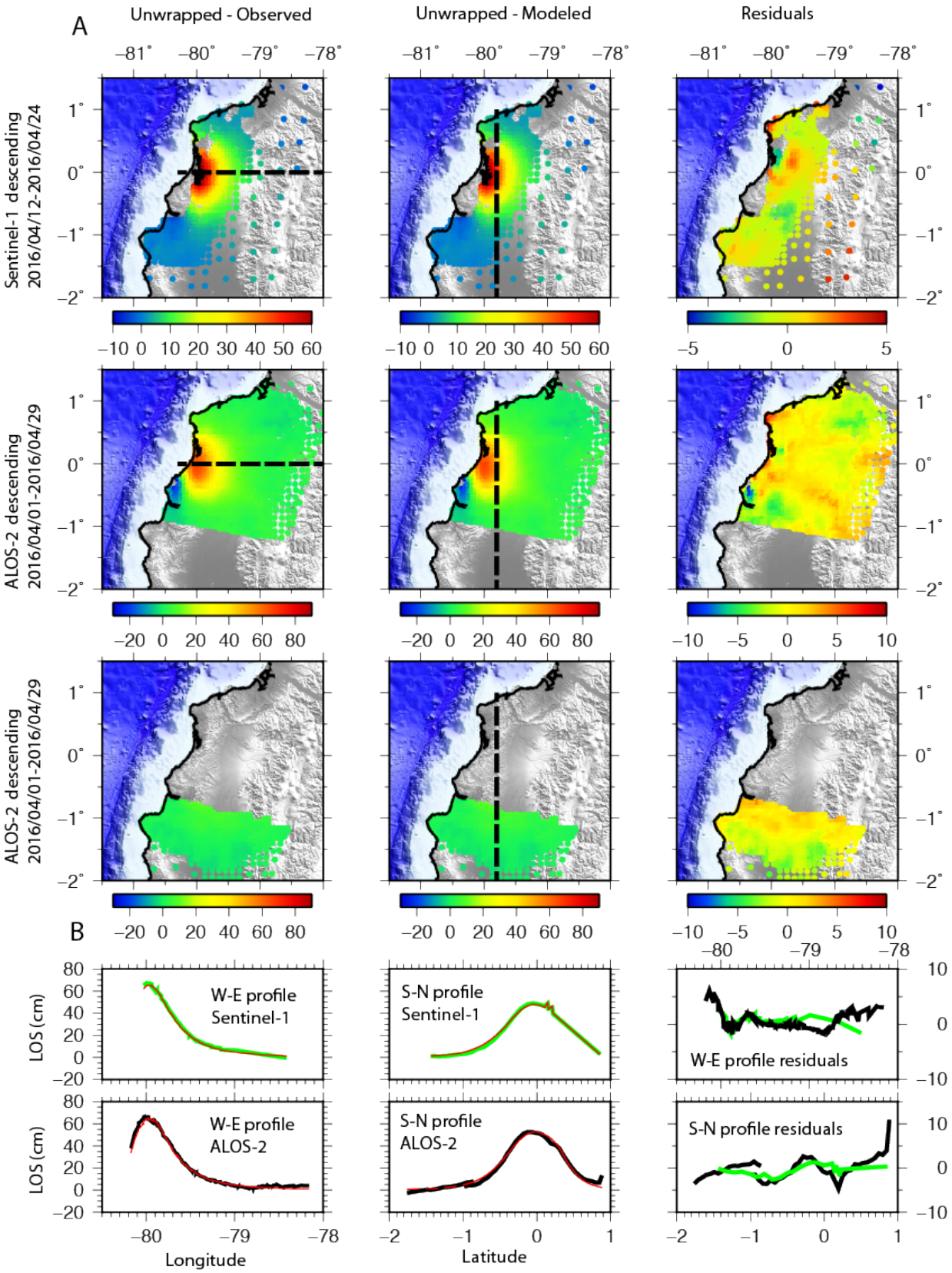
A
Unwrapped - Observed
Unwrapped - Modeled
Residuals
Sentinel-1 descending
2016/04/12-2016/04/24
ALOS-2 descending
2016/04/01-2016/04/29
ALOS-2 descending
2016/04/01-2016/04/29
B
W-E profile
Sentinel-1
S-N profile
Sentinel-1
W-E profile residuals
W-E profile
ALOS-2
S-N profile
ALOS-2
S-N profile residuals
LOS (cm)
Longitude
Latitude

Supplementary Figure 5 | Comparison between observed and modelled coseismic static displacement from unwrapped InSAR data. A. Line of sight (LOS) values for observed (left column), predicted (middle column) and residuals (right column). All values are in cm and color-coded according to the scale shown under each sub-figure. Satellite and acquisition dates are indicated on the left side of the figure. The dashed black line indicates the location of profile used in sub-figure B. B. Comparison of observed and predicted LOS coseismic displacements along the two profiles shown in A. The first two columns indicate observed LOS displacements for the unwrapped Sentinel-1 descending interferograms (green curve) and the two-part unwrapped ALOS-2 interferogram (black curve) together with the model prediction (red curve). The figure in the right column shows the residuals (Observed - Predicted) for each profile. Green and black lines are for Sentinel-1 and ALOS-2 data respectively.

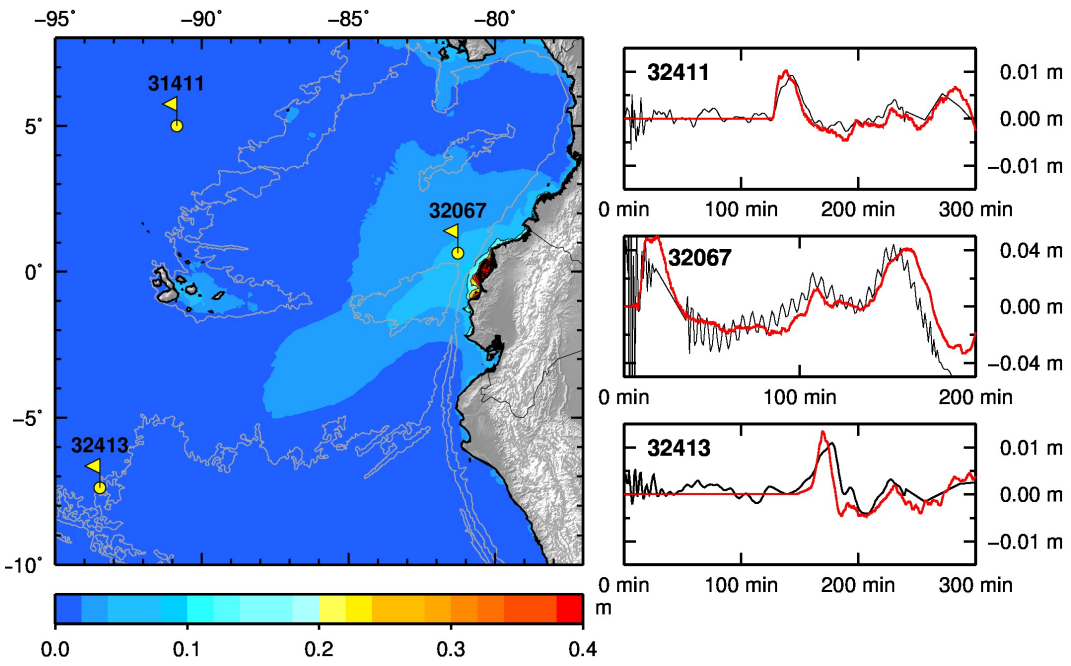

Supplementary Figure 6 | Comparison between observed and modelled tsunami signal induced by the 2016 Pedernales earthquake at three DART buoys. Left: location of the three DART buoys. Right: Observed (thin black line) and predicted (red line) water height changes during 300 mn after the earthquake time origin.

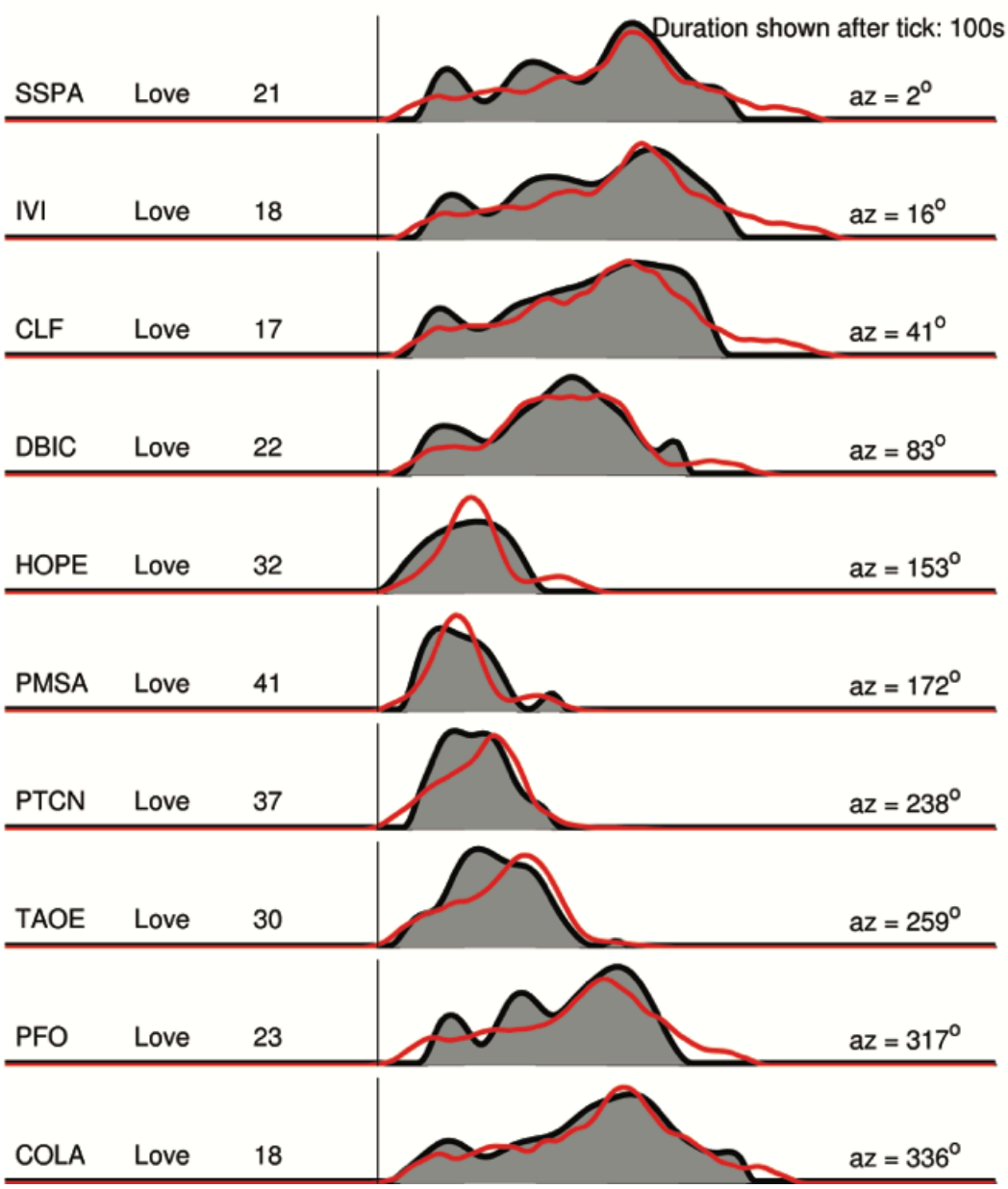

Supplementary Figure 7 | Comparison between observed (filled black curves) and Love-waves Relative Source Time Functions predicted from our kinematic slip model (red). For each station, its name, wave type, peak amplitude in 10^{18} Nm/s, and azimuth are indicated.

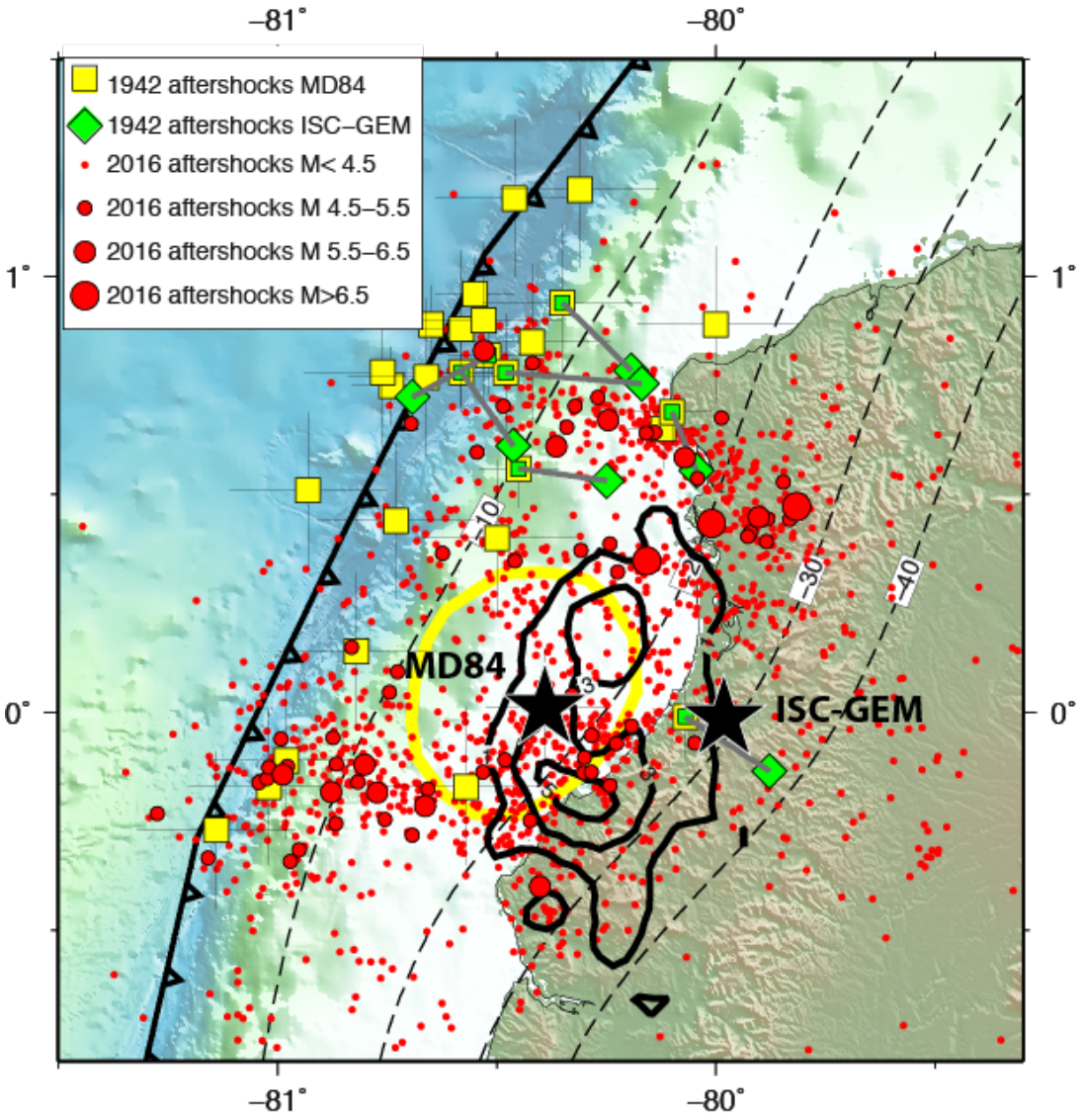

Supplementary Figure 8 | Aftershocks recorded during the 3 months following the 1942 and 2016 earthquakes. Location uncertainties for the 1942 aftershocks[2] (yellow squares) are showed by the thin black lines according to their quality determination. Green diamonds show the aftershocks relocated by the ISC-GEM catalogue[3] and the grey line indicates their location difference with ref 2. Aftershocks for the 2016 earthquake are from the Instituto Geofisico de la Escuela Politecnica Nacional, revised from http://www.igepn.edu.ec/mapas/mapa-evento-20160416.html. Black stars indicated the epicentres from ref 2,3.

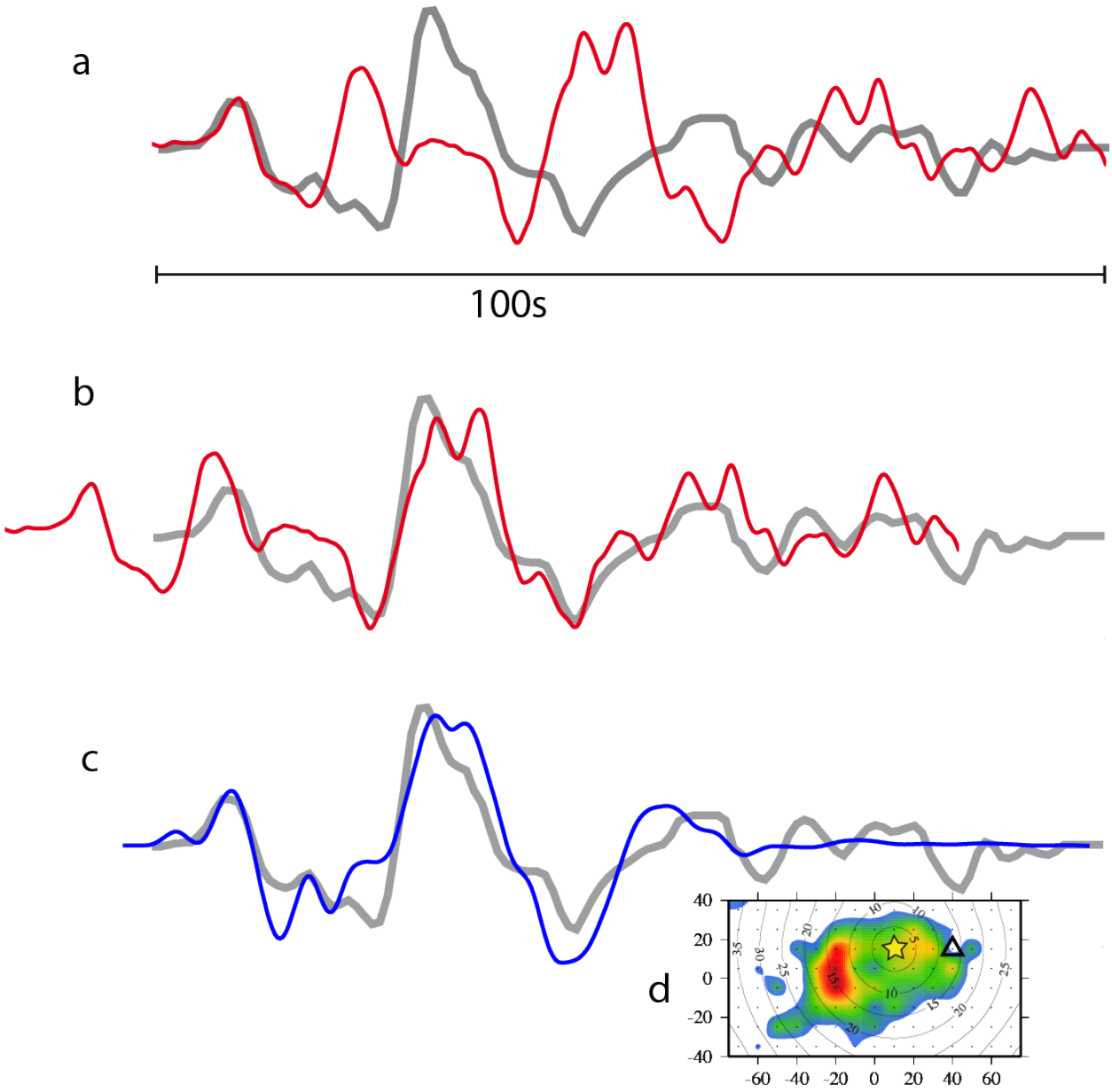

Supplementary Figure 9 | East component waveforms for the 1942 and 2016 earthquakes at DBN seismic station (The Netherlands). The thick grey curve is the original waveform digitized from ref 4. The red curve is the waveform observed for the 2016 earthquake. a. waveforms are aligned using the P wave arrival. b. Same as a, except that waveforms are now aligned using a shift of 15s maximizing their overall similarity. c. The blue curve shows the simulated waveforms obtained for a virtual earthquake using our 2016 slip distribution and rupture velocity of 2.3 km/s, but with a hypocentre (yellow start in the inset d) shifted 30 km SSW from its 2016 location (black triangle in the inset). Waveforms are aligned on the first significant P wave arrival. d. Rupture map for a virtual earthquake reproduced the 1942 waveform. Numbers and circles are rupture propagation isochrones every 5s, indicating a 25-30s rupture duration. The chosen epicentre is indicated by the yellow star and is close from the location proposed by ref 2,4.

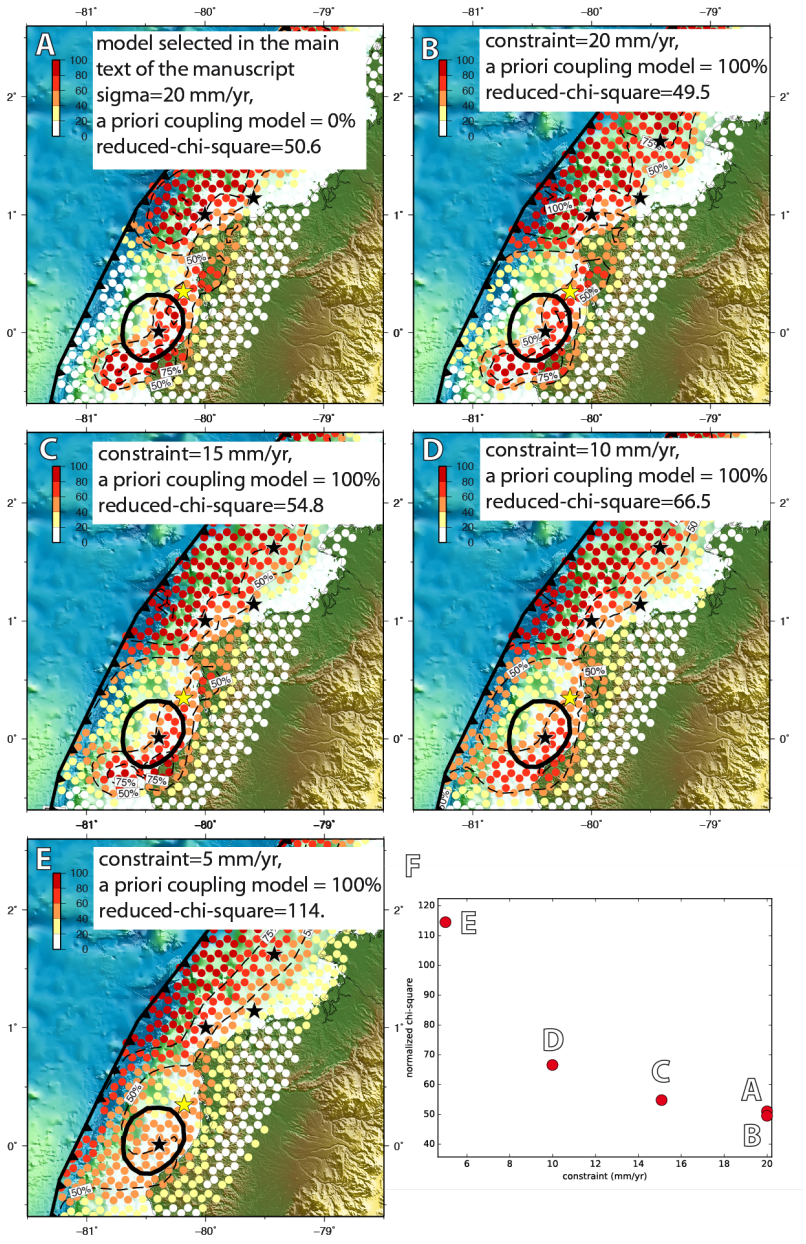

Supplementary Figure 10 | Test of maximum interseismic coupling (IC) allowed by GPS data along the Pedernales subduction segment. A. Model selected for figure 1 in the main text, obtained using a 20 mm/yr a priori constraint ($\boldsymbol{\sigma}$) with respect to a null coupling model ($\boldsymbol{m_0}$=0). B. Same as A but for a 100% coupling a priori model. C, D, E: same as B for a priori constraint of 15, 10, 5 mm/yr. F. Misfit (reduced chi-square) for models A-E. IC>40% is allowed by the GPS data very close to the trench without significant misfit increase (models C & D, 30% increase of the normalized chi-square), evidencing little resolution at the shallowest part of the subduction interface. Having significant IC (> 40%) west of the 2016 earthquake rupture degrades the fit by more than 100% (normalized chi-square 114 vs 50) and can therefore be

statistically rejected. Models A, B, C & D are allowed at the 95% confidence level. Their corresponding moment deficit rate is within the uncertainties indicated in the main text.

Site	Position		Coseismic Displacement (mm)			Uncertainty (mm)		
	Long.	Lat.	De	Dn	Du	SDe	SDn	SDu
ALTB	−78.55	0.91	−20.08	−7.15	5.89	1.87	2.40	4.92
ARSH	−79.10	0.10	−103.51	3.67	1.35	2.37	2.60	5.60
BAHI	−80.40	−0.66	−117.73	−260.28	146.80	2.82	2.54	2.42
CABP	−80.43	−0.39	−542.77	−633.80	514.33	2.18	3.03	1.80
CHIS	−80.73	−1.05	−14.54	−35.48	11.55	2.03	3.41	4.52
ECEC	−79.45	−0.27	−191.69	45.46	−20.31	3.39	2.48	3.13
ESMR	−79.72	0.93	−18.59	−12.18	−15.40	1.48	2.41	2.04
FLFR	−79.84	−0.36	−392.26	150.81	−134.29	2.87	3.16	4.97
GGPA	−78.59	−0.18	−54.49	7.28	−0.64	2.59	3.03	6.29
HSPR	−78.85	−0.35	−72.10	16.31	2.01	2.84	2.65	4.50
LGCB	−79.57	0.38	−189.92	−65.64	−35.81	2.66	2.34	5.19
LPEC	−79.16	1.09	−18.28	−7.31	−2.05	1.62	3.47	3.40
MOMP	−80.05	0.49	−104.39	−45.09	−50.27	1.84	2.82	5.26
ONEC	−80.10	−0.70	−68.55	4.67	−74.85	1.59	1.13	3.76
PDNS	−79.99	0.11	−680.41	−81.67	−216.39	1.99	2.23	3.94
PLHA	−78.50	0.02	−47.90	2.06	8.39	1.78	2.76	7.08
QUEM	−78.50	−0.24	−49.83	7.01	−0.28	1.62	3.11	9.00
QVEC	−79.47	−1.01	−50.93	34.73	−2.27	4.65	4.19	5.68
RVRD	−79.38	1.07	−16.27	−8.06	−12.09	2.09	3.20	6.50
SEVG	−80.03	−0.97	−28.35	11.51	−2.30	2.57	3.71	5.37
SNLR	−78.85	1.29	−15.52	−3.50	−3.99	0.73	0.71	2.27

Supplementary Table 1 | Coseismic displacements estimated from CGPS data. Long., Lat.: longitude, latitude in decimal degrees. De, Dn, Du: east, north and vertical coseismic displacement in mm; SDe, SDn, SDu: formal error (1-sigma confidence level) of De, Dn, Du.

Site	Position		Coseismic Displacement (mm)			Uncertainty (mm)		
	Long.	Lat.	De	Dn	Du	SDe	SDn	SDu
MUIS	−80.02	0.60	−75.15	−25.43	–	10.38	7.01	–
CHOR	−80.07	0.04	−750.76	−65.97	–	15.50	5.44	–
PPRT	−80.22	−0.13	−727.58	−106.69	410.61	15.02	7.03	10.23
BAHX	−80.41	−0.60	−188.38	−310.34	–	5.18	5.55	–
MANT	−80.67	−0.94	−42.25	−66.43	–	20.06	10.14	–
FLAX	−79.59	0.80	−51.36	−22.96	–	10.07	10.19	–
AGFR	−79.71	0.21	−442.56	−77.36	–	124.11	100.73	–
OLIM	−80.13	−0.71	−57.20	16.48	–	10.20	5.16	–
MINA	−80.28	−0.96	−22.49	−57.24	–	20.02	20.42	–
EPRS	−79.51	−0.59	−151.03	57.29	–	10.04	10.02	–
MER1	−79.51	−0.19	−237.28	35.46	–	10.07	10.05	–
MERC	−79.51	−0.19	−230.48	41.74	–	10.58	10.09	–

Supplementary Table 2 | Coseismic displacements estimated from GPS campaign data. Long., Lat.: longitude, latitude in decimal degrees. De, Dn, Du: east, north and vertical coseismic displacement in mm; SDe, SDn, SDu: formal error (1-sigma confidence level) of De, Dn, Du. Up

component could not be reliably estimated, except at site PPRT, a former CGPS site, re-occupied after the earthquake.

Top depth (km)	VP (km/s)	VS (km/s)	Density (kg/m^3)
0	3.39	1.96	1686
4.2	5.86	3.39	2553
27.5	8.07	4.66	3325

Supplementary Table 3 | Structure model derived from the waveform modelling of a Mw 5.2 earthquake (2010/11/25). This model is used for all the static offsets and waveform synthetics.

References

1. Hayes, G. P., Wald, D. J. & Johnson, R. L. Slab1.0: A three-dimensional model of global subduction zone geometries. *J. Geophys. Res. Solid Earth* **117,** (2012).
2. Mendoza, C. & Dewey, J. W. Seismicity associated with the great Colombia-Ecuador earthquakes of 1942, 1958 and 1979: implications for barrier models of earthquake rupture. *Bull. Seismol. Soc. Am.* **74,** 577–593 (1984).
3. Storchak, D. A. *et al.* The ISC-GEM Global Instrumental Earthquake Catalogue (1900-2009): Introduction. *Phys. Earth Planet. Inter.* **239,** 48–63 (2015).
4. Swenson, J. L. & Beck, S. L. Historical 1942 Ecuador and 1942 Peru subduction earthquakes, and earthquake cycles along Colombia-Ecuador and Peru subduction segments. *Pure Appl. Geophys.* **146,** 67–101 (1996).